Influence of precursor concentration on spray and particle formation in flame spray pyrolysis

Malte Bieber[1]*, Ricardo Tischendorf[2], Hans-Joachim Schmid[2], Manuel Reddemann[1], Reinhold Kneer[1]
[1]RWTH Aachen University, WSA, Institute of Heat and Mass Transfer, D-52062 Aachen, Germany
[2]Paderborn University, PVT, Particle Technology Group, D-33098 Paderborn, Germany
*Corresponding author: bieber@wsa.rwth-aachen.de

Abstract
Liquid atomization is expected to be a key process in Flame Spray Pyrolysis, as it determines the primary droplet size and velocity distribution, which represent initial conditions for flame shape and temperature field. A well-defined manipulation of atomization may be achieved by variation of nozzle geometry, injection parameter or fluid properties. However, change of fluid properties, e.g. varying solvents or increasing the precursor concentration, also influences the final particle properties.
In this work, the influence of precursor concentration on fluid properties, spray and particle formation in Flame Spray Pyrolysis is experimentally investigated. High-speed shadowgraphy and Phase-Doppler measurements are conducted in a semi-closed combustion chamber with a well-defined burner geometry (SpraySyn burner) that is based on a coaxial atomization principle.
By adding precursor to the flammable solvent, resulting spray characteristics, flame shape and appearance are changed in color, shape and mean droplet size distribution. Compared to resulting mean droplet sizes of pure solvent mixtures ($D_{32} \geq 22\,\mu m$), mean droplet sizes in the center of the precursor flame at 30 mm above the burner are generally smaller ($D_{32} \geq 18\,\mu m$). Persisting high share of small droplets in the droplet size distribution are presented, that presumably origin from an accumulation of metal organic precursor at the droplet surface during combustion, that acts as a diffusive barrier for high volatility solvent and thus reduces droplet evaporation.
Sufficiently high above the nozzle exit, increasing the precursor concentration does not affect the radial distribution of mean droplet sizes but leads to increased mean particle sizes. More precursor presumably leads to higher concentrations of prime particles in the flame, thus probability of particle collusion and agglomeration.
High-speed imaging at nozzle exit revealed random fluctuations of initial jet diameter, paired with jet axis shifting around $\sim$1000 Hz. These superposed fluctuations determine the initial conditions for atomization, induce pulsations in the flame and thus initiate the entire chain of the particle synthesis process.

Keywords
Flame Spray Pyrolysis, coaxial atomization, mean droplet size distribution, precursor concentration

Introduction

Flame Spray Pyrolysis (FSP) represents a liquid-feed aerosol flame synthesis of nanoparticles and is known for its flexibility in producing a wide range of nanoparticle powders with high purity [1]. Produced nanomaterials can consist of metals as well as single metal oxides and more complex mixed oxides [2] that are exemplarily utilized for catalysts, electroceramics (fuel cells, batteries), medicine (bio materials, diagnostics, drug delivery) or sensors [3] with superior functionality over conventional products [1]. However, the overall process complexity in the flame is very high: Particle characteristics are presumably determined in the flame within a few milliseconds residence time and influenced by various sub-processes including atomization and spray formation, droplet evaporation, flame chemistry and the particle formation [4]. The links between all sub-processes are not yet fully understood, which is required for being able to produce a more sophisticated product output with unique functionalities [5].
Industrial applications of FSP aim for maximum particle output and therefore prefer high concentration of precursor in the solvent. Though, high precursor concentrations directly influence the fluid properties, e.g. liquid viscosity and therefore the inlet conditions of the entire synthesis process chain [6]. Assuming constant injection parameters a variation of fluid properties directly influences primary breakup and resulting droplet phase. The droplet phase however represents the starting conditions for evaporation, combustion and thus the flame temperature field. Combustion and the resulting temperature field influence the synthesis process and ultimately the final output of nanoparticles. Commercial FSP systems (e.g. NPS10, Tethis S.p.A., Ital.) are based on coaxial atomization of the liquid precursor solution followed by pilot flame ignition. In this context, high relative velocities between gas and liquid phase result in high shearing, that imposes and amplifies initial jet instabilities and ultimately leads to jet disintegration during primary atomization [7]. The atomization process can be described as a superposition of primary and secondary instabilities of Kelvin-Helmholtz and Rayleigh-Taylor type [8]. Measurements of resulting fluctuations in breakup length, jet radius and radial jet tip position have been conducted in order to further characterize these instabilities regarding dependencies of operation parameter combinations on instability frequencies [9]. Despite profound investigations of coaxial atomization with generic nozzle designs, coaxial atomization is yet to be fully understood due to the high complexity of primary atomization phenomena but represents the basis of the entire

FSP process. Especially the influence of flame, initial fluid mixture and precursor solutions on atomization has not been investigated yet.
The present work aims for a deeper understanding regarding early stages of the process chain: the influence of FSP relevant precursor concentration on atomization and spray formation. Investigations are performed by comparing primary breakup and resulting droplet phase of pure solvents and precursor solutions. First, physical properties that are relevant for liquid atomization and applied measurement techniques are determined in dependency on precursor concentration, i.e. density ρ, viscosity ν, surface tension σ as well as refractive index n. On this basis, primary atomization is investigated by combining far-field microscopy and high-speed shadowgraphy for cold and hot conditions. The resulting radial and axial distributions of mean droplet size are characterized with standard Phase-Doppler technique. In addition, axial particle size distributions are measured above the flame with a scanning mobility particle sizer (SMPS) and are correlated with the obtained droplet data.

Material and methods

In order to identify and understand the relevance of precursor concentration on the overall process chain of FSP a three-step investigation is performed in this study. First, the influence of precursor on physical and optical properties is analyzed by measuring fluid viscosity, refractive index and surface tension for pure solvent, solvent mixture and varying precursor concentration. On this basis, the impact of physical property variations on atomization and spray formation is investigated by combining far-field microscopy and high-speed shadowgraphy directly at nozzle exit with downstream Phase Doppler measurements for droplet size distributions. Finally, the impact of precursor concentration and primary breakup on nanoparticle synthesis is evaluated by means of complementary data on mean particle sizes which are measured above the flame with a scanning mobility particle sizer (SMPS).
Burner, Injected fluids, material properties and injection parameter: For generation of the spray-flame, the standardized SpraySyn burner * [10] is utilized, based on a centered liquid jet, that is atomized by a coaxial dispersion gas flow, before it is ignited in a methane pilot flame (Figure 1). Standard operation parameter sets, that are used in this work, are presented in Table 2. The burner is embedded into a windowed hexagonal combustion chamber for full optical access. To ensure a continuous liquid mass flow feed, a dual rate syringe pump (KD Scientific Gemini 88) is utilized for liquid feed. The pilot flame is generated by directing premixed CH_4 and O_2 at $\lambda = 4$ through a porous sintered brass matrix, paired with pressured sheath air co-flow for matrix cooling and spray flame confinement. Measurements are performed with Iron(III)nitrate nanohydrate (>99% purity) as precursor, that is dissolved in either A: pure Ethanol ($\geq$ 99.8 % purity) or B: a mixture of 35 % Vol Ethanol and 65 % Vol 2-Ethylhexanoic acid (EHA - $\geq$ 99 % purity).

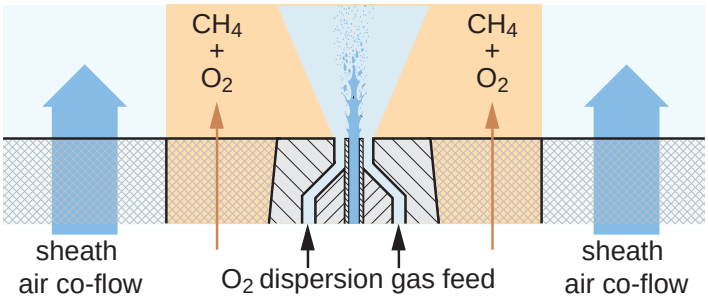

Figure 1. Schematic illustration of the SpraySyn burner. Liquid feed is provided through a centered cannula and atomized with a coaxial O_2 dispersion gas flow. The pilot flame is generated by directing premixed CH_4 and O_2 at $\lambda = 4$ through a porous sintered brass matrix. The resulting spray flame is confined by pressured air co-flow [10].

Pure gas cylinder Oxygen is used as dispersion gas. Two different operation conditions are investigated: Operation condition 1 with a low dispersion gas volume flow rate of V_g=5 slm for V_l=1.5 ml/s liquid feed rate and operation condition 2 with high dispersion gas volume flow V_g=10 slm for V_l=2 ml/s.
Material properties of Ethanol (A), mixture B and solutions of mixture B with Iron(III)nitrate nanohydrate are presented in Table 1. All physical properties are measured at 20 °C fluid temperature. For determination of viscosity ν an Ubbelohde viscosimeter is utilized and afterwards compared with data obtained via rotational viscosimetry. All fluids show Newtonian behavior. Measurements of density ρ and surface tension σ are conducted using the Krüss K100 force tensiometer. The refractive index n is measured with an Abbe refractometer DR-MR2.
Relevant non-dimensional numbers resulting from the parameter variation above and describing the atomizer operating flow conditions are the gas and liquid flow Reynolds number (Re_g, Re_l), gas Weber number We_g and gas-to-liquid momentum flux ratio (M).

$$Re_g = \frac{u_g \cdot 2 \cdot s}{\nu}, \qquad Re_l = \frac{u_l \cdot d}{\nu}, \qquad We_g = u_{rel}^2 \cdot \rho_g / \sigma, \qquad M = \frac{\rho_g \cdot u_g^2}{\rho_l \cdot u_l^2} \tag{1}$$

with the annular gap width s and the inner diameter d of the liquid feed capillary (see Figure 2, right).

Measurement setup and procedure:
The general test and measurement setup is presented in Figure 2 (left). For investigation of primary breakup and oscillating jet movements, high-speed videos are captured directly at nozzle exit (Fastcam SA-X, Photron Limited), as highlighted in Figure 2, right (black rectangle and shadowgraphy image). Frame rates of 40k fps at 768 x 376

*The SpraySyn burner represents a key component of the German Research Foundation priority program SPP1980 for synthesis of nanoparticles. Hence, two standardized operation parameter sets of the SpraySyn burner are investigated in this work to ensure comparability and to provide experimental data for numerical investigations of other participating research groups.

Table 1. Measured material properties (density ρ, kin. viscosity ν, surface tension σ and refractive index n) of A: Ethanol, B: mixture of 35% Vol Ethanol and 65% Vol 2-Ethylhexanoic acid and varying concentrations of Iron(III)nitrate nanohydrate dissolved in B.

		A	B	B + 0.1 mol/l	B + 0.2 mol/l	B + 0.3 mol/l
ρ	$[kg/m^3]$	789.50	867.83	903.14	973.78	1079.73
ν	$[m^2/s \cdot 10^{-6}]$	1.52	4.44	4.63	4.90	5.11
σ	$[N/m \cdot 10^{-6}]$	2.23	2.57	2.63	2.66	2.67
n	$[-]$	1.363	1.405	1.407	1.410	1.412

Table 2. Dimensionless quantities for operating conditions 1 (V_g=5 slm, V_l=1.5 ml/s) and 2 (V_g=10 slm, V_l=2 ml/s) at nozzle exit for coaxial atomization with A and B representing the liquids as described in Table 1.

Flow conditions	u_g	u_l	Re_g	Re_l	We_g	M
A1	60.3	0.20	3580	52	93	166
A2	120.6	0.27	7159	70	370	374
B2	120.6	0.27	7159	23.9	322	340
B2 + 0.1	120.6	0.27	7159	22.9	315	327
B2 + 0.2	120.6	0.27	7159	21.7	311	302
B2 + 0.3	120.6	0.27	7159	20.8	309	273

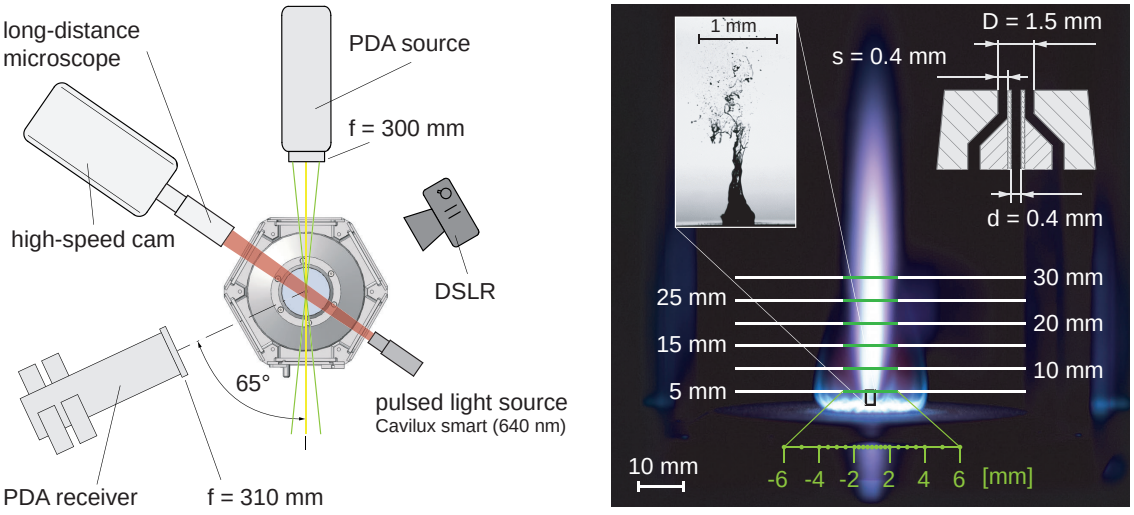

Figure 2. Left, experimental setup for spray investigation of coaxial gas stream driven atomization. Characterization of the dispersed phase is conducted regarding velocities and mean diameter using Phase-Doppler technique. For investigation of primary breakup high-speed shadowgraphy is utilized with a long-distance transmitted light microscope and a monochromatic low-coherence pulsed light source. Right, a macroscopic image of the spray flame is presented including the investigated positions for Phase-Doppler measurements (green lines and dots). Additionally, the region of interest for high-speed shadowgraphy is presented at nozzle exit (black rectangle).

pixel resolution and 80k fps at 512 x 224 pixel resolution are used with 195 px/mm, resulting in 3.9 mm x 1.9 mm and 2.6 mm x 1.15 mm frame size. To minimize motion blur, a monochromatic and incoherent pulsed light source (Cavilux Smart, 640 nm wavelength, 10 ns pulse duration) is used for back-light illumination. In addition, conventional photography by means of digital conventional single-lens reflex (DSLR) imaging is utilized for qualitative visualization of the flame.

Droplet sizes are determined with Phase-Doppler technique (source: ILA 2D fp50 LDV System with 250 mW at 532 nm and 561 nm; receiver: DANTEC PDA Classic, BSA P80 processor). The receiver is positioned for observation at scattering angle of 65° in order to minimize the influence of potential refractive index variation in the flame caused by evaporation of more volatile components in the solvent mixture [11]. The combustion chamber is mounted on a combination of three linear translation stages that move in x,y and z-direction with a minimum increment of 0.1 mm. As indicated with green lines in Figure 2, the spray flame is scanned at specific heights above the burner ($5 \leq$ HAB $\leq$ 30 mm) and in radial direction from -6 mm to 6 mm with decreasing increment towards the center.

Resulting mean nanoparticle sizes are measured with a scanning mobility particle sizer (SMPS) for data comparison of droplet phase data with resulting particle size distribution. However, extraction of gas samples in and above the flame for particle measurements is challenging. Due to thermophoresis, chemical reaction and agglomeration, particle properties along the measuring section can change abruptly within a few milliseconds and before any probe

reaches the SMPS. Therefore, all gas samples for particle measurements are extracted with a "Hole in a Tube" probe sampling system (HiaT-system), to quench the sample immediately at the sampling position in the flame and suppress particle growth. Probes are diluted to a concentration of 10^5 #/cm^3, which suggests a representative sampling based on quenching aerosol dynamics [12] and preliminary conducted investigations.

Results and discussion

Investigation of the mutual influence of precursor concentration on spray and particle formation is performed by comparing spray formation of pure solvents with multiple precursor solutions with varying concentration. For this purpose, microscopic high-speed shadowgraphy is conducted for visualization of primary breakup phenomena and Phase-Doppler measurements are performed for a quantitative characterization of the resulting droplet phase.

Fluctuation of jet diameter and jet axis position at nozzle exit: In Figure 3 left, exemplary microscopic high speed images of the primary breakup region of Ethanol is shown for M = 166 (V_g = 5 slm, V_l = 1.5 ml/s). Images 2-6 represent exemplary microscopic images at different time steps of the same injection process. In white, a scaled schematic drawing of the nozzle outlet geometry is highlighted. By comparing the jet contour with the orifice geometry, two distinct jet fluctuations can be identified: fluctuation of the jet outlet diameter directly at nozzle exit and the position of the jet center axis relative to the orifice center axis.

Fluctuation of jet outlet diameter: As exemplarily shown in image 6, the jet exit diameter does not match the nozzle orifice diameter. Instead, the jet is widened due to additional spreading of liquid on the flat top of the needle tip, presumably due to capillary force driven surface wetting. However, the resulting diameter is not constant but varies over time (cf. images 5 and 6). Without dispersion gas (not shown here), the liquid phase spreads over the entire nozzle tip as a result of force equilibrium between gravitation and capillary force driven spreading and surface tension induced contraction. The diameter with active dispersion gas is in the range of nozzle orifice diameter (see

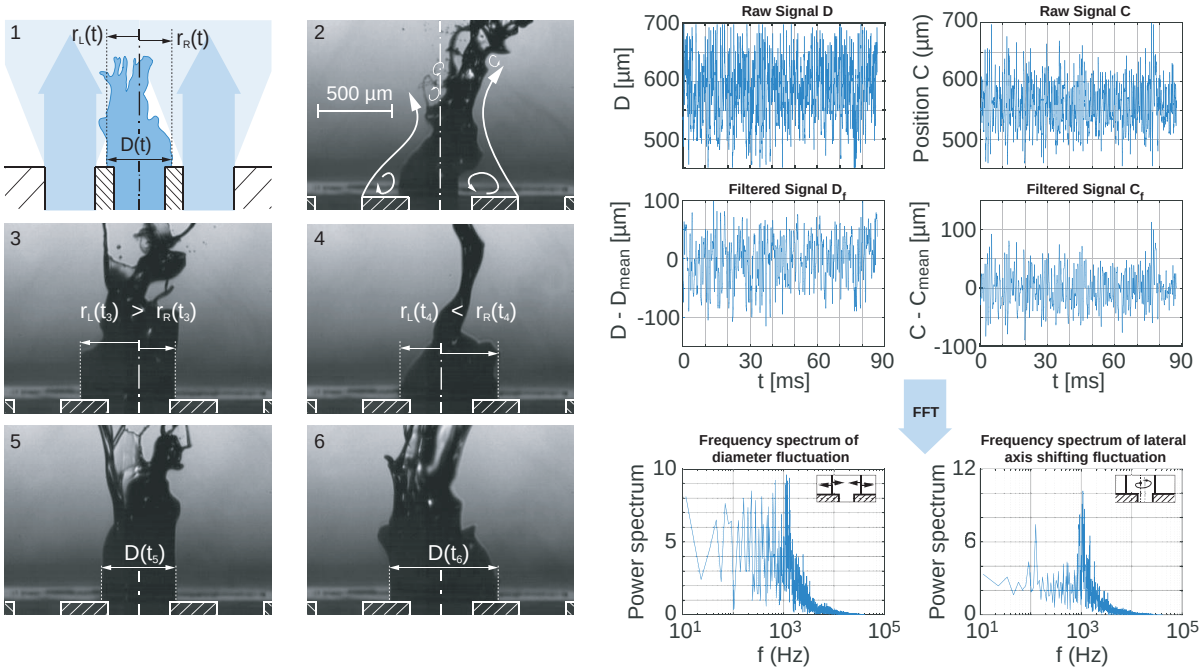

Figure 3. Left, microscopic high speed images at nozzle exit of the ignited Ethanol spray flame at M = 166 (V_g=5 slm, V_l=1.5 ml/s). Right, measured jet diameter at nozzle exit, jet center position over time and Fast Fourier transform of the signal for characterization of dominant jet fluctuation frequencies.

images 5 and 6). With active dispersion gas, an additional retracting force needs to be considered: gas pressure induced forces are acting on the liquid surface and actively push it back and forth.

Lateral shift of the jet center axis: A second fluctuation of the jet can be observed in lateral direction as shown in images 3 and 4. Lateral fluctuation in 2d-images could be either a side shift of the jet or caused by a circumferential movement. In order to quantify fluctuations of the jet diameter and jet axis shifting directly at nozzle exit, the images are further evaluated numerically. An edge detection algorithm is applied to identify the positions of the liquid interface (left interface position $r_l(t)$ and right interface position $r_r(t)$, in order to calculate the jet diameter $D(t)$ and center position $C(t)$ at nozzle exit:

$$D(t) = r_r(t) - r_l(t) \qquad C(t) = \frac{r_r(t) + r_l(t)}{2} \tag{2}$$

In Figure 3 top right, the corresponding raw data of $D(t)$ and $C(t)$ is shown over time for subsequent data processing. A median filter is applied to the raw data in order to attenuate noise by averaging over 10 adjacent time steps. Evaluated videos are captured at a framerate of 80 kfps. After median filtering, frequencies of up to 4 kHz can be identified in the data signal. Resulting frequency power spectra for $D(t)$ and $C(t)$ are obtained by applying Fast Fourier transforms (FFT) to the attenuated signals. The FFT of $D(t)$ show no distinct peak in the frequency spectrum, leading to the conclusion that diameter fluctuations are random. Even though peaks in the frequency spectrum of $C(t)$ can be distinguished, present peaks are overall low, wide spread in the same order of magnitude. However, the highest peak and multiple lower side peaks are concentrated around 1 kHz. Consequently both fluctuation types are presumably imposed mainly by turbulence of the expanding gas phase.
Fluctuating movements of the jet directly at nozzle exit can be described as a superposition of high frequency tangential and/or radial jet shifting and pulsation of jet diameter. These effects are assumed to be imposed by the gas phase. Commonly described instabilities in the context of coaxial atomization, e.g. Kelvin Helmholtz type instabilities, are usually present further downstream but not directly at nozzle exit. Therefore, the three described types of fluctuation can only be explained by additional forces that are caused by radial and/or tangential velocity components in the gas phase directly at nozzle exit. Consequently, additional velocity components presumably develop during nozzle internal gas flow or directly at nozzle exit. In this context, numerical simulations of internal nozzle flow would be a promising approach for clarification but have not been performed in this work.
An oscillating jet diameter directly at nozzle exit could also be caused by a pulsating mass flow rate. Such a pulsation would not be assumed initially since the utilized syringe pump for liquid feed ensures a constant mass flow into the injection system. Hence, fluctuations of mass flow must develop somewhere between injection system inlet and nozzle exit. A potential cause for fluctuations in liquid mass flow could be flow separation of the gas flow at nozzle exit or nozzle internal turbulence in the gas phase. Immediately after leaving the annular gap, the gas flow expands until it interacts with the liquid jet as described above. Low static pressure regions caused by corner flow and gas phase acceleration can cause suction which potentially forces liquid to be dragged out of the capillary faster than the liquid feed of the syringe pump. The needle would then have to be continuously refilled until suction takes over again. As shown in Figure 3 image 2, the effect of suction can lead to states in which the jet diameter is smaller than the inner capillary diameter. The described effect of suction can also be followed by circulation of the gas into the needle and the development of stagnation point pressure above nozzle exit, both acting as a barrier for liquid flow. As a result in high-speed images of the flame glowing, strong flame pulsation is visible at all times.
Liquid properties (e.g. ν, ρ and σ) potentially affect fluctuation in jet diameter and therefore the initial conditions for atomization, spray and flame formation. A comparison of these fluctuations in dependency on fluid properties needs to be conducted in future investigations.

Determination of the radial and vertical region of interest: In Figure 4, mean droplet sizes and droplet size distributions are compared for different axial and radial positions inside the spray flame. Exemplary axial measurement positions are shown in Figure 4 a), i.e. HAB = 5, 15 and 30 mm. For definition of the radial region of interest, radial measurement data rate distribution is used as shown in subfigure b) for HAB = 30 mm, i.e. position of maximum spray and flame width. Note, that highest data rates are obtained in the region $0 \leq r \leq 1$ mm. In the region $1 \leq r \leq 4$ mm, the data rate decreases rapidly until it drops below 100 Hz for $r \geq 4$ mm. Data evaluation is conducted for $-3 \leq r \leq 3$ mm. In Figure 4 c), D_{10} and D_{32} at spray-flame center ($r = 0$ mm) are plotted over HAB for solvent mixture (B) and precursor solution. For HAB $\geq$ 5 mm, D_{10} and D_{32} decrease with increasing HAB until a minimum is reached at HAB = 10 mm for D_{10} and at HAB = 15 mm for D_{32}. Further downstream (HAB > 15 mm), both mean diameter values continuously increase for all following investigated heights above burner. After primary and secondary atomization are completed, evaporation and combustion remain as prime mechanisms for changes in droplet sizes and thus mean diameters. Due to the well known radius-square-law, small droplets evaporate faster than bigger droplets. Hence from HAB = 15 mm to 30 mm, small droplets presumably evaporate completely, leading to generally increased values of D_{10} and D_{32} along the center axis.
In Figure 4 d),e),f), arithmetic (D_{10}) and Sauter (D_{32}) mean diameter for pure Ethanol, solvent mixture B and precursor solution spray flames are presented over radial position r for HAB = 5, 15 and 30 mm. For HAB = 5 mm, the radial distribution of D_{10} is similar for all investigated fluids and can be described as funnel shaped with a flattened minimum in the center. Radial distributions of D_{32} show two local minima at $r = -1$ mm and $r = 1$ mm with a local maximum in the center ($r = 0$ mm) for all investigated fluids. Unlike for HAB = 5 mm, all distributions of mean diameter for HAB = 15 mm have a single distinct minimum in the center position and increase in radial direction. These basic changes of distribution shape for D_{32} are paired with a decrease of center region values from $D_{32}(r = 0) = 22.5$ µm to $D_{32}(r = 0) = 17$ µm. However, the values of D_{10} remain similar compared to the upstream position HAB = 5 mm with minima within the range of $6 \leq D_{32} \leq 7$ µm. Towards the downstream position HAB = 30 mm the general shape of mean diameter distributions remains similar, but flattens by means of increased values in the center and decreased values at the outer edges in radial direction for Ethanol and solvent mixture B. Concluding, the radial distributions of mean diameters further indicate that primary and secondary atomization appear to be completed at HAB = 15 mm for all investigated liquids. Further downstream (HAB $\geq$ 15 mm), evaporation and combustion remain as prime mechanisms for changes in droplet sizes and radial distribution of mean diameters. From HAB = 15 mm to 30 mm, small droplets presumably evaporate completely, which leads to generally increased values of D_{10} and D_{32} in the center, where small droplets are more frequent compared to the outer jet regions ($r \geq 2$ mm). For $r \geq 2$ mm mean diameter values decrease with increasing HAB, since evaporation and shrinking of large droplets paired with disappearing small droplets are dominant.

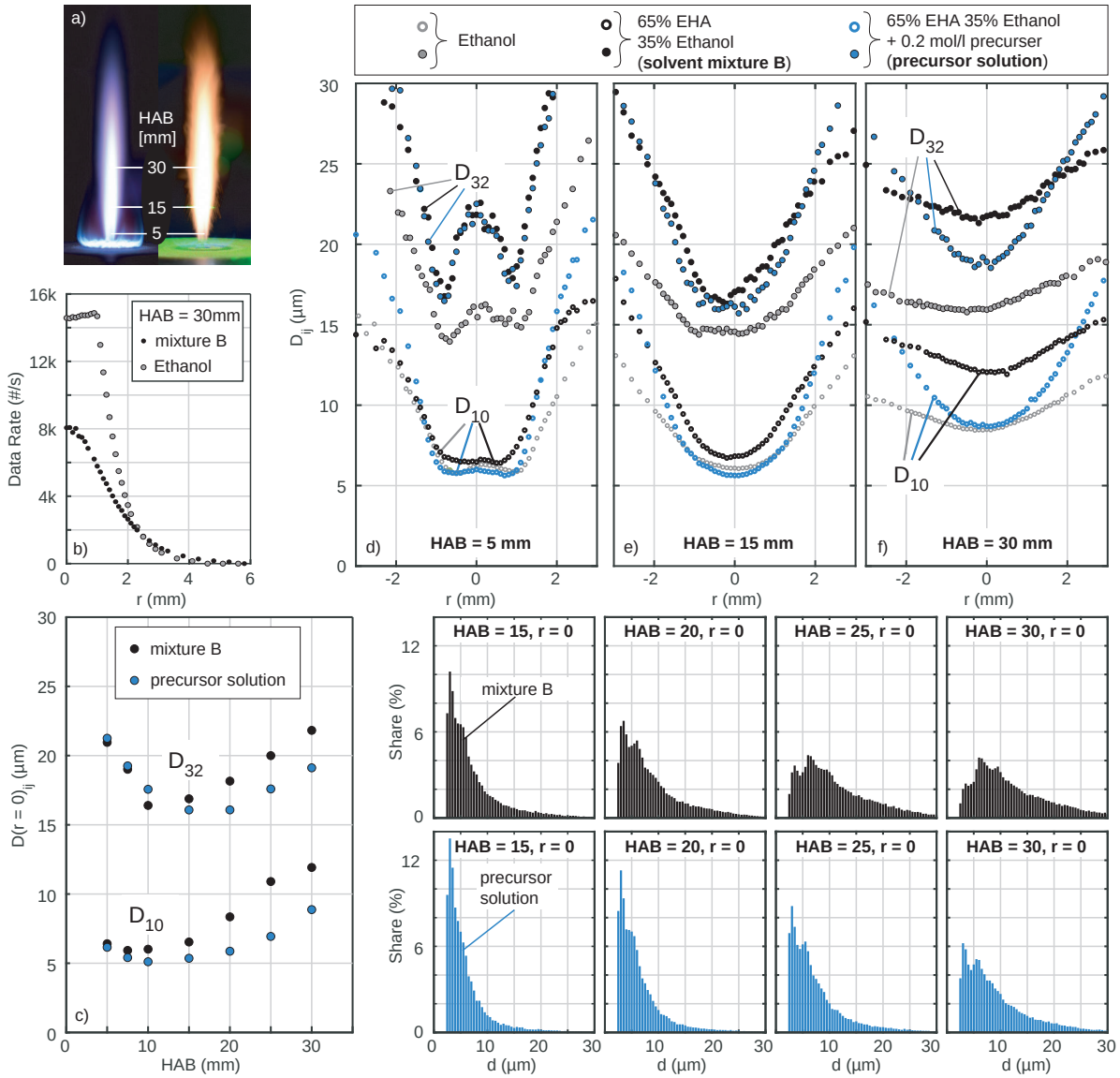

Figure 4. a) Qualitative flame images of pure solvent (left) and precursor solution (right) at operating parameter set 2 (V_g=10 slm, V_l=2 ml/s) with axial measurement positions (HAB). b) Measurement data rate over radial measurement position for HAB = 30 mm. c),d),e), Arithmetic (D_{10}) and Sauter (D_{32}) mean diameter over radial position at HAB = 5, 15 and 30 mm for Ethanol, solvent mixture (B) and precursor solution. f) D_{10} and D_{32} at spray-flame center (r = 0 mm) over HAB for solvent mixture (B) and precursor solution. Bottom right, droplet size distribution at r = 0 mm for mixture B and precursor solution at multiple HAB.

Influence of precursor addition on qualitative flame shape and droplet size distribution: In Figure 4 from e) to f), general shape of the radial mean diameter distribution in the precursor flame does not significantly change from HAB = 15 mm to HAB = 30 mm compared to resulting mean diameter distributions of pure solvent mixture B. As described above, the mean diameter distribution of solvent mixture (B) flattens by means of increased values in the center and decreased values at the outer edges. For precursor solution, the general shape of mean diameter distribution remains identical from HAB = 15 mm to 30 mm, but with increased values in the region $-2 \leq r \leq 2$ mm. Comparing D_{10} of precursor solution with mixture B, the increase in arithmetic diameter between HAB = 15 mm and 30 mm is significantly lower in the center region for precursor solution, along with a significant increase in the measured data rate from $\sim 8000\,\#$/s to $\sim 12000\,\#$/s. Hence, more small droplets appear to be present despite evaporation.

Bottom right in Figure 4, two sets of droplet size distributions are presented at r = 0 mm, $15 \leq$ HAB ≤ 30, i.e. downstream of the primary and secondary atomization region. The top set shows droplet size distributions for solvent mixture (B) and below, resulting droplet size distributions in the precursor solution spray flame are presented. For solvent mixture (B) at HAB = 15 mm, the droplet share exponentially decreases towards increasing droplet sizes. Thereby, the maximum is in the range of 2 µm $\leq$ d $\leq$ 3.5 µm, i.e. close to minimum diameter for Phase-Doppler measurement technique [13]. Towards HAB = 30 mm, the share of small droplets decreases and the main peak shifts towards bigger droplets (5 µm at HAB = 30 mm) as well as the overall shape of the droplet size distribution, since small droplets completely evaporate and thus the share of bigger droplets increases. For the precursor solution at HAB = 15 mm, the droplet share exponentially decreases towards increasing droplet sizes as well but steeper, due

to higher share of small droplets. This high share of small droplet is in good agreement to Figure 4 e) and f), in which the center values of mean diameters are always smaller for the precursor solution compared to solvent mixture without precursor. Analogous to the findings for solvent mixture (B), the share of small droplets decreases with increasing HAB, but at a slower rate for precursor solution. As a result, the peak of droplet share in the diameter range of 2 µm $\leq$ d $\leq$ 3.5 µm is still prominent at HAB = 30 mm. According to [14], during combustion of precursor solution high volatile solvent vaporizes in the flame and causes an accumulation of metal organic precursor at the droplet surface. This accumulation acts as a diffusive barrier for high volatility solvent inside the droplet, which could be a plausible explanation for increased downstream share of small droplets. Whether this effect is accompanied by a change of flame temperature caused by addition of precursor to the solvent needs to be investigated in future studies.

Influence of increasing precursor concentration on resulting mean droplet and particle sizes: In Figure 5, the influence of precursor concentration on spray and particle formation in the spray flame is presented. The first two figures show dependencies of D_{10} and D_{32} on radial position for HAB = 5 mm and 25 mm. Thereby, mean droplet diameters are similar for all fluids in the center region, but slightly diverge towards increased diameters for higher precursor concentrations with $r \geq 1.5$ mm. Hence, for the investigated range of precursor concentration in the solvent, no significant effects on mean droplet diameters can be observed. As stated above, the addition of precursor leads to smaller droplets. Concluding, once precursor is added to the solvent mixture, increasing the precursor concentration has no measurable effect on mean droplet sizes in the flame core. The third figure shows resulting

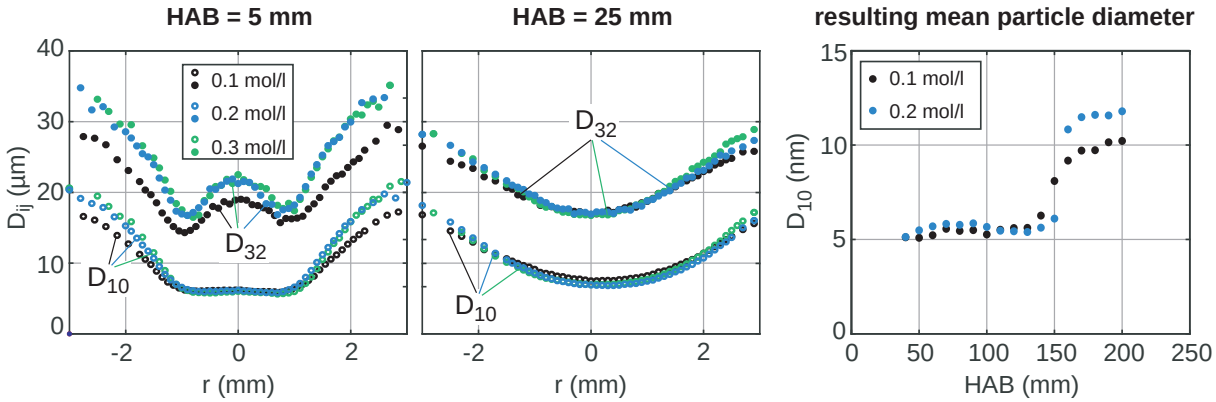

Figure 5. Left, arithmetic (D_{10}) and Sauter (D_{32}) mean diameter over radial position for varying precursor concentrations diluted in solvent mixture B at HAB = 5,and 25 mm (burner operation parameter: V_g=10 slm, V_l=2 ml/s). Right, arithmetic mean diameter of resulting nanoparticles in dependency on HAB (burner operation parameter V_g = 10 slm, V_l = 2 ml/s).

arithmetic mean particle diameters over HAB. Average mean particle sizes continuously increase with HAB due to downstream particle agglomeration. However, with higher precursor concentration, the mean diameter distribution is shifted towards larger particle sizes. Hence, despite identical mean droplet size distributions, increased precursor concentration in the droplet phase alone represents a sufficient initial condition for the development of larger particle agglomerates. Increasing the precursor concentration leads to more nucleation and thus higher densities of prime particles. Naturally, more particles increase the probability of particle collusion, agglomeration and ultimately lead to larger particle agglomerates.

Conclusions

Investigation regarding the influence of precursor addition and varying precursor concentration on the spray flame synthesis of nanoparticles has been performed. Therefore, the primary breakup, axial and radial distribution of mean droplet diameter and axial distribution of mean particle sizes has been analyzed.

Varying precursor concentration close to saturated solvent mixtures has shown little effect on the spray formation but influences resulting size of particle agglomerates. Regarding spray and flame formation, the addition of precursor always induces a change in flame appearance, e.g. light emission from the flame is changing into a bright yellow presumably due to glowing iron oxide particles and changed flame chemistry. In addition, the share of small droplets remains increased for all downstream measurement positions. During combustion of precursor solution high volatility solvent vaporizes in the flame and presumably causes an accumulation of metal organic precursor at the droplet surface that acts as a diffusive barrier. In this case, evaporation would be attenuated resulting in a persisting share of small droplets.

At HAB = 25 mm, i.e. post primary and secondary atomization, no significant changes in mean droplet diameter have been observed for varying precursor concentrations. Nevertheless, for all HAB investigated, mean agglomerate sizes increase with increased precursor concentration. More precursor and similar droplet size distributions lead to more particles in the early synthesis stages, which increases the probability of downstream particle collision in the particle aerosol phase, that ultimately amplifies agglomeration. Thresholds need to be identified for maximum

precursor concentration, at which more precursor does not further affect the spray formation. Therefore investigations with significantly lower precursor concentrations are required, sufficiently far from any state of saturation. However to date, the influence of initial droplet size distribution on flame formation and particle synthesis is not fully understood. Therefore, profound investigations with varying burner operation parameter are necessary, that will be included in future studies.
Conducted microscopic high-speed imaging of primary atomization at nozzle exit revealed two fluctuating liquid jet movements, that influence primary atomization and consequently spray formation. Capillary force driven surface wetting causes the liquid jet to spread directly at nozzle exit. After exiting, the liquid jet immediately expands over the needle tip and exceeds the inner needle diameter. However, opposing force induced by surface tension and pressure force that is imposed from the dispersion gas push back the liquid. As a result, the liquid jet diameter and the jet axis position relative to the needle axis are fluctuating over time directly at nozzle exit. Evaluation of high-speed imaging has been performed exclusively for pure ethanol. Investigation of precursor influence on fluctuations directly at nozzle exit have not been performed yet and are therefore subject of future investigations.

Acknowledgements
Gefördert durch die Deutsche Forschungsgemeinschaft (DFG) - KN 764/20-1, SCHM 1429/13-1.
Funded by the Deutsche Forschungsgemeinschaft (DFG, German Research Foundation) – KN 764/20-1, SCHM 1429/13-1

Nomenclature

ν	kin. viscosity [m^2/s]	s	annular gap width [m]
ρ	density [kg/m^3]	M	gas-to-liquid momentum flux ratio
σ	surface tension [N/m]	V_l	liquid volume flow rate [ml/s]
d	diameter [m]	V_g	gas volume flow rate [slm]
D	diameter of dispersion gas orifice [m]	HAB	Height above burner [mm]
f	frequency [Hz]	Re	Reynolds number [-]
f	focal length [m]	We	Weber number [-]
u	velocity [m/s]		

References

[1] Strobel, R., Pratsinis, S.E., 2007, *Journal of Materials Chemistry*, 17 (45), pp. 4743-4756.
[2] Thiebaut, B., 2011, *Platinum Metals Review*, 55 (2), pp. 149-151.
[3] Andronescu, E., 2017, “Micro and Nano Technologies”. Elsevier Science
[4] Kammler, H. K., Mädler, L., Pratsinis, S. E., 2001, *Chemical Engineering and Technology*, 24, (6), pp. 583–596.
[5] Stark, W.J., Pratsinis, S.E., 2007, *Powder Technology*, 126 (2), pp. 103-108.
[6] Noriler, D., Rosebrock, C. D., Madler, L., Meier, H.F., Fritsching, U., 2014, *Atomization and Sprays*, 24 (6), pp. 495–524.
[7] Marmottant, P., Villermaux, E., 2004, *Journal of Fluid Mechanics*, 498, pp. 73-111.
[8] Bieber, M., Menzel, S., Thiebes, A.L., Gabriel, C., Jockenhoevel, S., Kneer, R., Reddemann, M.A., Sep. 6.-8. 2017, 28th European Conference on Liquid Atomization and Spray Systems.
[9] Kumar, A., Sahu, S., 2018, *International Journal of Spray and Combustion Dynamics*, 10 (3), pp. 211–230.
[10] Menser, J., Kluge, S., Wiggers, H., Dreier, T., Schulz, C., 2015, *European Combustion Meeting*.
[11] Pitcher, G., Wigley, G., Saffman, M., 1991, *Applications of Laser Techniques*, pp. 227-247.
[12] Zhao, B., Yang, Z., Wang, J., Johnston, Murray V.; Wang, H., 2003, *Aerosol Science and Technology*, 37 (8), pp. 611-620.
[13] Fdida, N., Blaisot, J.B., Floch, A., Dechaume, D., 2008, 22nd European Conference on Liquid Atomization and Spray Systems.
[14] Li, H, Rosebrock, C.D., Wu, Y., Wriedt, T., Mädler, L., 2019, *Proceedings of the Combustion Institute*, 37, (1), pp. 1203-1211.